RESEARCH MEMORANDUM

INVESTIGATION OF LIFT AND CENTER OF PRESSURE OF LOW-ASPECT-RATIO, CRUCIFORM, TRIANGULAR, AND RECTANGULAR WINGS IN COMBINATION WITH A SLENDER FUSELAGE AT HIGH SUPERSONIC SPEEDS

By Thomas N. Canning and Billy Pat Denardo

Ames Aeronautical Laboratory
Moffett Field, Calif.

NATIONAL ADVISORY COMMITTEE
FOR AERONAUTICS

WASHINGTON

June 26, 1952

 CONFIDENTIAL

NATIONAL ADVISORY COMMITTEE FOR AERONAUTICS

RESEARCH MEMORANDUM

INVESTIGATION OF LIFT AND CENTER OF PRESSURE OF LOW-ASPECT-RATIO, CRUCIFORM, TRIANGULAR, AND RECTANGULAR WINGS IN COMBINATION WITH A SLENDER FUSELAGE AT HIGH SUPERSONIC SPEEDS

By Thomas N. Canning and Billy Pat Denardo

SUMMARY

Tests were conducted in the Ames supersonic free-flight wind tunnel to evaluate the usefulness of available theory for the calculation of lift-curve slope and center of pressure of low-aspect-ratio, triangular, and rectangular cruciform wings in combination with a long slender body. Tests were made in the range of Mach numbers between 1.3 and 6.2 and at Reynolds numbers from 2.8 million to 16.0 million based on model length. The results show that theoretical calculations give the lift-curve slope near zero lift within the experimental scatter and the center of pressure within about 3 percent of the body length. The variation of minimum drag coefficient with Mach number is presented for both models. Estimates based on experimental values of lift-curve slope and drag indicate that the triangular wing-body combination is the more efficient and may develop a lift-drag ratio of 4.5 at a Mach number of 6.0 for power-on operation, neglecting body-base drag.

INTRODUCTION

Many tests of wings and wing-body combinations have been made and the results compared with linear and more exact theories in the Mach number range below 3. In the Mach number range above 3, on the other hand, there are very few comparisons available (references 1 and 2). The present investigation is intended to provide some data for low-aspect-ratio, triangular, and rectangular cruciform configurations in this speed range at Reynolds numbers corresponding to a 10-foot-long missile flying between 80,000 and 100,000 feet altitude. The usefulness of available theory is investigated by comparing the calculated and experimentally determined aerodynamic coefficients in the range of Mach numbers from 1.3 to 6.2. The range of Reynolds numbers based on body length was 2.8 million at

M = 1.3 to 16.0 million at M = 6.0. The effect of Reynolds number on the aerodynamic coefficients was investigated at M = 6.0.

SYMBOLS

a	horizontal projection of the instantaneous acceleration of the model center of gravity normal to the tunnel center line, feet per second squared
C_D	drag coefficient $\left(\frac{D}{Sq_o}\right)$
$C_{D_{min}}$	drag coefficient at zero lift
C_L	lift coefficient $\left(\frac{L}{Sq_o}\right)$
C_m	pitching-moment coefficient about model center of gravity $\left(\frac{\text{pitching moment}}{Sq_o l}\right)$
C_{L_α}	lift-curve slope $\left(\frac{dC_L}{d\alpha}\right)$, per degree
C_{m_α}	pitching-moment-curve slope $\left(\frac{dC_m}{d\alpha}\right)$, per degree
D	drag, pounds
e	Naperian base
E,F	constants defining variation of α with time
f	frequency of the pitching motion, cycles per second
I	principal moment of inertia about lateral axis through model center of gravity, foot-pound seconds squared
K	ratio of two-dimensional lift-curve slope of airfoil calculated with shock-expansion theory to that calculated with linear theory
k	damping constant, per second
l	model length, feet
L	lift, pounds
m	model mass, slugs

M	test Mach number
q_o	free-stream dynamic pressure, pounds per foot squared
Q	double integral with respect to time of the angle of attack function, seconds squared
R	Reynolds number based on model length and free-stream conditions
S	maximum cross-sectional area of model body, feet squared
t	time, seconds
v	horizontal projection of the instantaneous velocity of model center of gravity normal to tunnel center line, feet per second
$X_{c.g.}, X_{c.p.}$	distance from model nose to center of gravity and center of pressure, respectively, feet
y	horizontal distance from tunnel center line, feet
α	angle of attack of model relative to local flight path, degrees
ω	$2\pi f$

Subscripts

1,2,3,4	refer to times, positions, and velocities at the instants of exposure of the shadowgraphs in stations 1, 2, 3, and 4, respectively
12,14, 23, etc.	refer to intervals between stations 1 and 2, 1 and 4, 2 and 3, etc.

EXPERIMENTAL TECHNIQUES AND MODELS

Facility

The experiments were performed in the supersonic free-flight wind tunnel of the Ames Aeronautical Laboratory. This facility is a short ballistic range within a variable pressure, supersonic, blowdown wind

tunnel. Details of tunnel design and operation are given in reference 3. The features of the facility pertinent to the present investigation are mentioned below.

The model is fired from a smooth-bore gun located in the wind-tunnel diffuser. As it passes upstream through the 15-foot-long test section 7 shadowgraph pictures, 4 in the horizontal plane and 3 in the vertical plane, are made. A chronograph records the instants of exposure of the shadowgraphs, completing a time history of the model position. Two typical shadowgraphs are shown in figure 1.

Methods of Measuring Aerodynamic Coefficients

General description.- The model is designed to execute between one-half and one and one-quarter pitching oscillations in the test section and is disturbed at launching so as to oscillate with an amplitude of about 5° in the horizontal plane. Small oscillations in the vertical plane result from accidental disturbances. The complete motion in 3 dimensions cannot be studied because of inadequate data in the vertical plane. Instead, the projection of the motion in the horizontal plane is used, assuming that the interaction between pitch and sideslip is negligible.

The aerodynamic coefficients are calculated from the record of model motion as a function of time. For an example of such data, see figure 2. Two methods have been used for determining lift-curve slope, pitching-moment-curve slope, and center-of-pressure position, C_{L_α}, C_{m_α}, $X_{c.p.}$, from the behavior of models oscillating in pitch. One method consists of measuring the flight-path curvature due to lift and the other consists of measuring the change in pitching-moment-curve slope resulting from large center-of-gravity shifts.

Lateral-movement method.- This method uses flight-path curvature as a measure of lift. Using Newton's second law of motion, the instantaneous acceleration of the center of gravity of the model normal to the tunnel axis may be written as follows:

$$a = \frac{d^2y}{dt^2} = \frac{C_{L_\alpha}\, \alpha\, q_o S}{m} \qquad (1)$$

This equation assumes a linear lift curve and neglects the contributions of the drag force, and the lift force due to pitching and plunging. These contributions are usually, but not always, negligible so care was exercised to see that the omissions were permissible. The direction of the lift force is, by definition, perpendicular to the flight path, but

the maximum observed inclination of the flight path relative to the tunnel axis was 0.5°. The error in the experimentally determined lift introduced here is given by the cosine of 0.5° and is therefore small.

The time variation of angle of attack in equation (1) can be obtained using the angle-of-attack measurements from the shadowgraph pictures and two assumptions which define the form of the motion. The assumptions are that the restoring moment is directly proportional to the angle of attack and the damping moment is directly proportional to the pitching and plunging rates. This leads to a variation of angle of attack given by

$$\alpha = e^{-kt} (E \cos \omega t - F \sin \omega t) \tag{2}$$

Equation (2) is fitted to the observed variation of α with respect to time by a least-squares procedure described in reference 4. In this way, the four unknowns, ω, k, E, and F, are evaluated. The complete set of 4 shadowgraphs is required to determine the sine wave so the method of least squares is not strictly required but is used as a convenient and systematic method.

Combining equations (1) and (2) gives the instantaneous lateral acceleration as a function of time:

$$\frac{d^2y}{dt^2} = \frac{dv}{dt} = \frac{C_{L_\alpha} q_o S}{m} e^{-kt} (E \cos \omega t - F \sin \omega t) \tag{3}$$

Integrating with respect to t gives the following equation for lateral velocity as a function of time:

$$v = \frac{dy}{dt} = v_1 + \frac{C_{L_\alpha} q_o S}{m} \int_{t_1}^{t} e^{-kt} (E \cos \omega t - F \sin \omega t) dt \tag{4}$$

in which v_1 is the lateral velocity at the first station. A second integration gives the equation of lateral displacement. The integrals are evaluated between limits corresponding to the times and lateral positions in two shadowgraph stations.

$$y_2 = y_1 + v_1(t_2 - t_1) + \frac{C_{L_\alpha} q_o S}{m} \int_{t_1}^{t_2} \int_{t_1}^{t} e^{-kt} (E \cos \omega t - F \sin \omega t) dt\, dt \tag{5a}$$

The double integral on the right can be evaluated since both the integrand and the limits are known. For brevity, it will be designated Q_{12}.

$$y_2 = y_1 + v_1(t_2 - t_1) + \frac{C_{L_\alpha} q_o S}{m} Q_{12} \tag{5b}$$

In this equation, the unknowns are C_{L_α} and v_1. The constant v_1 can be eliminated by using data from the third station:

$$y_3 = y_1 + v_1(t_3 - t_1) + \frac{C_{L_\alpha} q_o S}{m} Q_{13} \tag{5c}$$

Solving equations (5b) and (5c) simultaneously yields the following expression for C_{L_α}:

$$C_{L_\alpha} = \frac{m}{Sq_o} \frac{y_{12} - y_{13}(t_{12}/t_{13})}{Q_{12} - Q_{13}(t_{12}/t_{13})} \tag{6}$$

The least-squares fit to the variation of angle of attack with time establishes the pitching frequency f. This makes it possible to obtain the pitching-moment-curve slope about the center of gravity from the relation

$$f = \frac{1}{2\pi}\sqrt{\frac{-C_{m_\alpha} Sq_o l}{I}} \quad \text{or} \quad C_{m_\alpha} = -\frac{4\pi^2 f^2 I}{Sq_o l} \tag{7}$$

The center of pressure can be obtained from the lift and pitching-moment results using the relation:

$$\left(\frac{X_{c.p.} - X_{c.g.}}{l}\right) C_{L_\alpha} = -C_{m_\alpha} \tag{8}$$

Pitching-moment method.- The relation between lift-curve slope, center of pressure, and pitching-moment-curve slope given in equation (8) suggests that tests be made of similar models with widely separate centers of gravity. Solving equation (8) simultaneously for two such tests determines the unknowns C_{L_α} and $X_{c.p.}$ since C_{m_α} for each test is given by equation (7). This method has also been used in this investigation.

The lateral-movement method is inherently more accurate than the pitching-moment method for this facility and yields much smaller scatter in C_{L_α}. Both methods give reliable results for center of pressure, but the lateral-movement-method results contain less scatter here also. Values of C_{L_α} obtained with both methods are presented subsequently, but the values of $X_{c.p.}/l$ from only the lateral-movement method are presented.

Drag.- From the time history of the model position, deceleration and hence drag were determined. These calculations are based on the

assumption that C_D is constant. Details of this part of the data analysis are included in reference 3. Since, in these tests, angles of attack larger than 8.0° were sometimes observed, the varying drag due to lift was important. The effect of this varying drag, although not treated exactly, was accounted for approximately by subtracting from the indicated average value of C_D an approximate value of drag due to lift given by the mean value during test of (1/57.3) $C_{L_\alpha} \times \alpha^2$.

Models

The models were wing-body combinations and were constructed of various metals chosen to give the desired weights and center-of-gravity positions. The bodies were cone cylinders of fineness ratio 15 with a nose length of 6 body diameters. Wings of triangular and rectangular plan form were used. The aspect ratio of the exposed-wing panels joined together was 0.64. The profiles were of constant thickness except for bevelled leading edges; the constant thickness resulted in a constant airfoil section of 0.051 thickness ratio for the rectangular wing and a thickness ratio varying from 0.026 at the root to 0.160 at the tip on the triangular wing. This design compromise was accepted to reduce cost of the models, and it is believed that the lift and center-of-pressure results would not have differed significantly if the same airfoil section had been used on both models. Detailed sketches of the models are shown in part (a) of figure 3 and photographs are presented in figure 4.

The models were fired from a smooth-bore 20-mm. gun and were held in plastic sabots designed to give support and to impart a pitching disturbance to the model at separation. A sketch of a typical sabot is given in figure 3(b), and a photograph is presented in figure 4. The pitching motion resulting from this initial disturbance was recorded as described above to give the data required. As may be seen in figure 3(b) and figure 4, the models left the gun with an initial angle of attack, and the plane of this angle was parallel to the plane of the 4-shadowgraph group.

THEORETICAL CALCULATIONS

Theoretical values of lift-curve slope and center of pressure of each configuration were calculated at several points within the Mach number range. An approximate theory similar to that of Nielsen (references 5 and 6) was used for both configurations. In the reference papers, the approach is to combine the calculated lift of the various parts of the model alone and the lift induced on each part by the others. The load distribution on the body alone is calculated using slender-body

theory. The lift distribution on the two exposed wing panels joined together is estimated using Stewart's paper (reference 7) for the triangular wing and the paper by Lagerstrom (reference 8) for the low-aspect-ratio rectangular wing. The lift induced on the wings by the body upwash field is estimated using the slender wing-body theory of Spreiter (reference 9). The point of application of this lift component is taken as the center of pressure of the two wing panels joined together. The lift induced by the wing on the body and its point of application are estimated by reducing the problem to the planar case in a manner similar to that developed by Morikawa (reference 10). Superposition of these components of lift and pitching moment gives the desired estimates of C_{L_α} and $X_{c.p.}/l$.

In the present investigation, a modified theory was used in which four departures from the method as described were made, as suggested in reference 5, in order to make the theoretical flow correspond more closely with the real flow. The lift on the nose of the body was calculated using Kopal's tables (reference 11), and the lift carry-over from the nose onto the cylindrical portion of the body was evaluated by means of Tsien's paper (reference 12), using the exact rather than the approximate relation between local velocity and pressure. In calculating the lift carry-over onto the body from the wing, the fact that these models have no body aft of the wing was accounted for approximately. In addition, in the case of the rectangular wing, the sum of lift on the rectangular wing and the lift on the body due to the presence of this wing was increased by accounting for the fact that the flow consisted of a shock-wave expansion flow instead of the Mach wave type of flow assumed in reference 6. This was done by multiplying this part of the lift by the ratio

$$K = \frac{C_{L_\alpha}\text{S.E.}}{C_{L_\alpha}\text{L.T.}}$$

in which C_{L_α}S.E. is the lift-curve slope of the actual profile in two-dimensional flow calculated using shock-expansion theory, and C_{L_α}L.T. is the same quantity calculated using linearized theory. This procedure was used in reference 2. The theoretical contribution of each part of the configurations to the lift is presented in figure 5. The net effect on the estimated lift-curve slope of the rectangular-wing model introduced by the four modifications is large at high Mach numbers.

RESULTS AND DISCUSSION

The experimental variation of C_{L_α} with Mach number for the two models is given in figures 6 and 7 for both types of analysis of the same

test firings. Comparison of the two sets of results indicates a fair consistency between the two methods except that the lateral-movement method yields somewhat lower values of C_{L_α} at the higher Mach numbers and yields less scatter at all Mach numbers. For purposes of discussion, the results of only the lateral-movement analysis will be considered because of the apparent advantage in accuracy. The small number of data points on these plots results from the requirement that displacements from a straight flight path of 0.15 inch or greater must be observed in order to obtain reliable answers. One possible explanation of the remaining scatter in these results is described in the appendix. The values of C_{L_α} predicted using the modified theory were within the apparent band of experimental scatter of ± 9 percent from the median value for both models at all Mach numbers at which tests were made. This indicates that existing theoretical results are of value in this Mach number range for simple configurations.

The experimentally determined centers of pressure, obtained by the lateral-movement method, were usually forward of the predicted positions as shown in figure 8. The maximum discrepancies between experiment and theory were observed on one model of each type at $M = 4.5$; in each case the discrepancy was about 5 percent of the body length. The forward movement of the center of pressure with increasing speed was well predicted.

The tests show that the rectangular wing exhibits slightly superior effectiveness as a stabilizer for the test body both because its center of pressure is farther aft and because it has a higher lift-curve slope. This superiority is gained at the expense of a large drag increase over that of the triangular wing as is shown in figure 9. This figure presents the variation with Mach number of the zero-lift drag, $C_{D_{min}}$, of both models.

Although direct measurement of lift and drag at constant angle of attack was not possible in this investigation, a comparison of lift-drag ratios was made based on the assumptions that

$$C_L = C_{L_\alpha}\alpha$$

and

$$C_D = C_{D_{min}} + \frac{1}{57.3} C_{L_\alpha}\alpha^2$$

neglecting the lift and drag of whatever trimming device might be chosen. The angles of attack for maximum lift-drag ratios at $M = 6.0$ were 7.5° or less. Since the amplitude of oscillation of the test models was

usually about 5.0°, it is felt that extrapolation to 7.5° should not introduce important errors in the comparisons. When the value of $C_{D_{min}}$ was taken to be the total measured value at zero lift, the attainable lift-drag ratios of the two models at $M = 6.0$ are 4.0 and 3.4 for the triangular and rectangular wing models, respectively, at corresponding lift coefficients of 1.4 and 1.7.

To estimate the performance which might be realized in power-on operation, the drag was reduced by subtracting the estimated body-base drag (base pressure assumed equal to 0.3 of the free-stream static pressure). This assumption is conservative as judged from the data of reference 13 although the Mach number range of the reference test was somewhat lower. The triangular-wing model again appeared more efficient having, at $M = 6.0$, an $(L/D)_{max}$ of 4.5 at $C_L = 1.2$, as compared to an $(L/D)_{max}$ of 3.6 at $C_L = 1.6$ for the rectangular-wing model. These values of attainable lift-drag ratios are considered encouraging in view of the fact that extreme aerodynamic efficiency was not the basis for design. The comparative efficiencies of the two models might be altered somewhat by using the same airfoil section on both models, but the changes from the present results would probably be small.

The results of tests indicated no measurable effect of Reynolds number on the lift-curve slope, center of pressure, or drag of the models at $M = 6.0$ in the range of Reynolds number from 5.3 to 16.0 million. This corresponds to a Reynolds number range based on mean exposed chord of 1.2 to 3.6 million.

CONCLUDING REMARKS

The theory of Nielsen (references 5 and 6), when altered to account for the effects of airfoil section, lift carry-over from the nose onto the cylindrical portion of the body, and the absence of an afterbody, predicts values of C_{L_α} within the experimental scatter and the mean center-of-pressure positions within about 3 percent of the body length for both models at Mach numbers between 1.5 and 6.0.

Although the rectangular wing is slightly more effective than the triangular wing as a stabilizer for the test body, estimates of the lifting efficiency of the two models indicate that the triangular wing is superior as a lifting surface. Estimates of the lift-drag ratios for power-on operation with no allowance for the effects of a trimming device indicate that values as high as 4.5 may be attained at a Mach number of 6.0.

Ames Aeronautical Laboratory,
National Advisory Committee for Aeronautics,
Moffett Field, Calif.

APPENDIX

APPARENT SCATTER IN C_{L_α}

The method of data analysis described in the body of the report is based on the assumption of linear pitching-moment characteristics. Experimental results for many similar configurations indicate seriously nonlinear characteristics at large angles of attack. Since the present investigation was restricted to small angles, nonlinearities probably did not contribute important errors in the results, but may have introduced some scatter. Such pitching-moment characteristics are frequently well represented by the expression

$$C_m = C_{m_\alpha}\alpha + \text{constant } \alpha^3$$

Assuming this in the present case, the oscillatory motion resulting from an initial disturbance is complicated, but it may be seen that since the restoring moment is disproportionately large at high angles of attack the peaks will be sharper than in the case of a sine wave of the same frequency and amplitude.

Assume that the actual oscillation is given in the sketch by the solid line

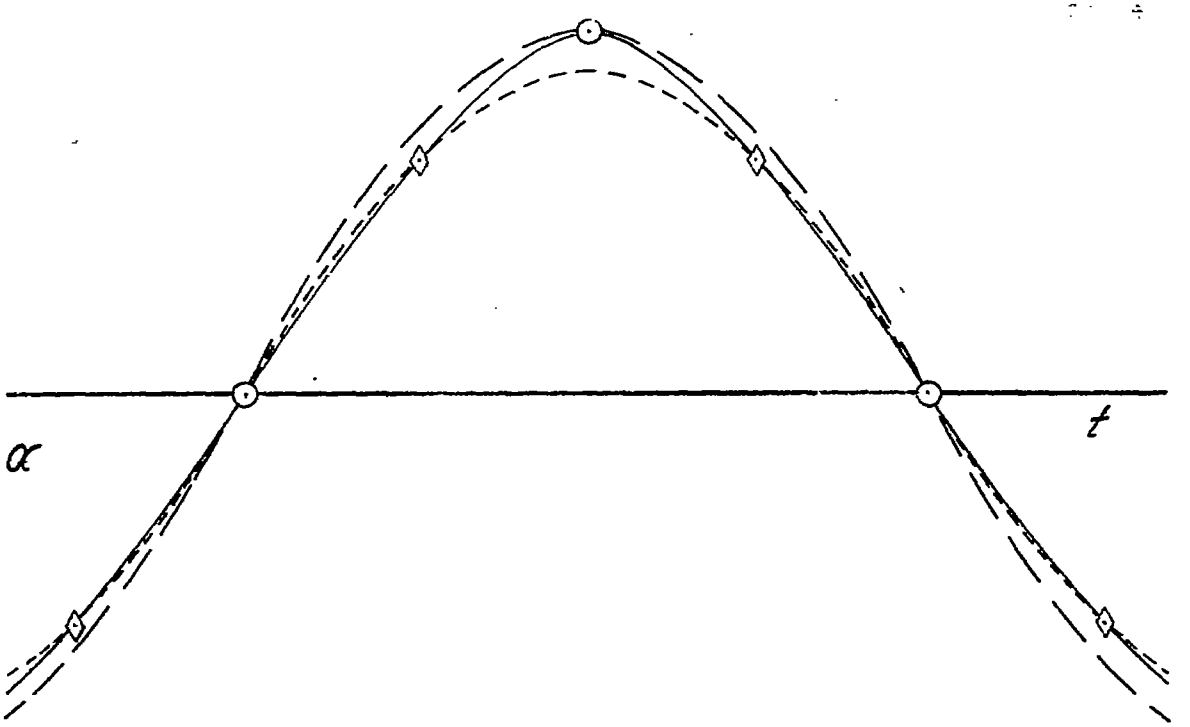

Consider first that the positions of the shadowgraph images correspond to the circled points. If a sine wave is passed through these points, indicated by the dashed curve, it is seen that the area under each loop of the sine wave is significantly larger than the area under the actual curve. Since the lift-curve slope is obtained by comparison of the lateral movement of the model to the integration of this curve twice with respect to time, as described in the body of the report, it may be seen that the values of Q in equation (6) will be too large and the analysis will underestimate the average lift-curve slope. On the other hand, if the shadowgraphs correspond to the $\diamond$ points, the lift-curve slope will be overestimated.

The results of an examination of all test runs for conditions at which duplicate data was obtained support the above contention. Two tests which fitted the pattern for underestimation, including each type of model, gave decidedly low answers. Similarly, three tests which fitted the pattern for overestimation gave decidedly high answers. Nine tests, which fitted neither pattern, either agreed well with one another or gave results which fell inside the scatter of other runs.

Three tests did not agree with the correlation. Two of the three did not fit either pattern and gave high answers. The amplitude of pitching oscillation in one of these cases was small and the accuracy of measuring y may not have been sufficient; the pitching amplitude in the other case was greater than 10° and may have gone into the seriously nonlinear lift-curve range. The third test fitted the pattern for underestimation and gave a high answer. The pitching amplitude in this last case was small enough to indicate that accuracy of measuring y may again have been marginal.

It is believed that the errors introduced by the nonlinearities discussed above do not seriously impair the value of the experimental results. The median point of the scatter probably represents quite well the average value of lift-curve slope over the experimental range of angle of attack.

REFERENCES

1. McLellan, Charles H., Bertram, Mitchel H., and Moore, John A.: An Investigation of Four Wings of Square Plan Form at a Mach Number of 6.86 in the Langley 11-Inch Hypersonic Tunnel. NACA RM L51D17, 1951.

2. McLellan, Charles H.: Exploratory Wind-Tunnel Investigation of Wings and Bodies at M = 6.9. Jour. Aero. Sci., vol. 18, Oct. 1951, pp. 641-648.

3. Seiff, Alvin, James, Carlton S., Canning, Thomas N., and Boissevain, Alfred G.: The Ames Supersonic Free-Flight Wind Tunnel. NACA RM A52A24, 1952.

4. Shinbrot, Marvin: A Least-Squares Curve-Fitting Method With Applications to the Calculation of Stability Coefficients From Transient-Response Data. NACA TN 2341, 1951.

5. Nielsen, Jack N., and Kaattari, George E.: Method for Estimating Lift Interference of Wing-Body Combinations at Supersonic Speeds. NACA RM A51J04, 1951.

6. Kaattari, George E., Nielsen, Jack N., and Pitts, William C.: Method for Estimating Pitching-Moment Interference of Wing-Body Combinations at Supersonic Speed. NACA RM A52B06, 1952.

7. Stewart, H. J.: The Lift of a Delta Wing at Supersonic Speeds. Quart. Appl. Math., vol. 4, no. 3, Oct. 1946, pp. 246-254.

8. Lagerstrom, P. A., and Graham, Martha E.: Low Aspect Ratio Rectangular Wings in Supersonic Flow. Douglas Aircraft Co. Rept. SM-13110, Dec. 1947.

9. Spreiter, John R.: Aerodynamic Properties of Slender Wing-Body Combinations at Subsonic, Transonic, and Supersonic Speeds. NACA Rep. 962, 1950. (Formerly NACA TN 1662)

10. Morikawa, George: The Wing-Body Problem for Linearized Supersonic Flow. Ph.D. Thesis, CIT, Calif., 1949.

11. Mass. Inst. Tech., Dept. Elec. Engr. Tables of Supersonic Flow Around Yawing Cones. By the Staff of the Computing Section, Center of Analysis, under the direction of Zdenek Kopal. Tech. Rep. No. 3, Cambridge, 1947.

12. Tsien, Hsue-Shen: Supersonic Flow Over an Inclined Body of Revolution. Jour. Aero. Sci., vol. 5, no. 12, Oct. 1938, pp. 480-483.

13. Kurzweg, H. H.: Interrelationship Between Boundary Layer and Base Pressure. Jour. Aero. Sci., vol. 18, no. 11, Nov. 1951, pp. 743-748.

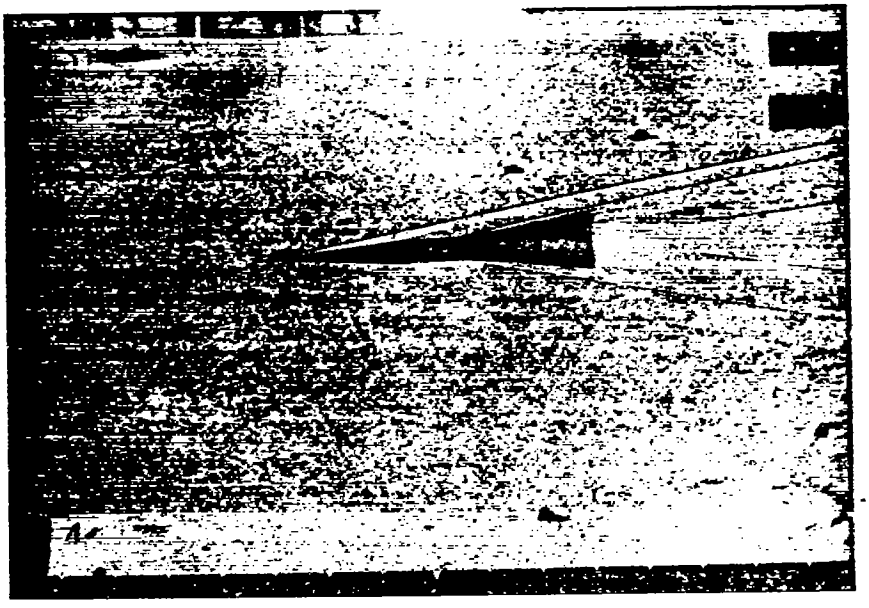

(a) Triangular-wing model, $\alpha = -3.0^{\circ}$.

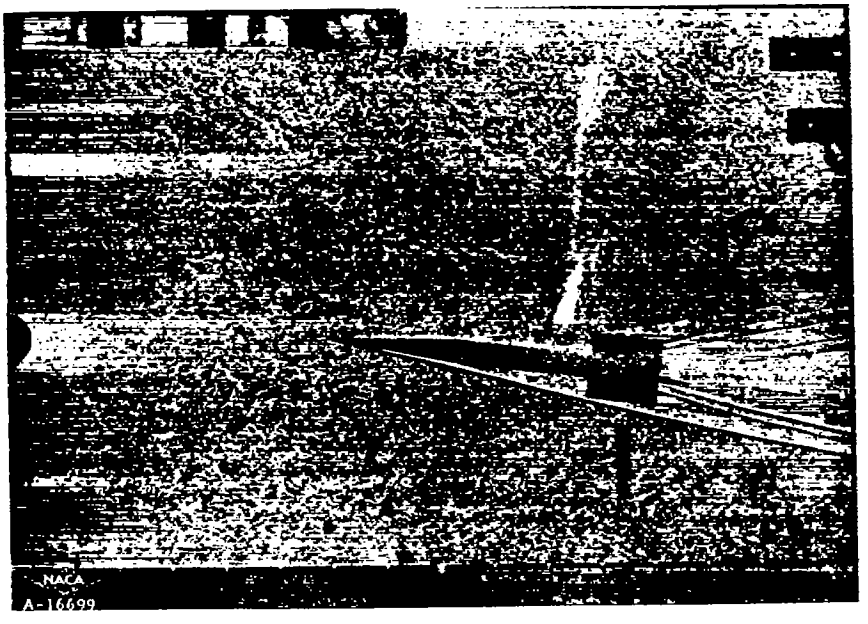

(b) Rectangular-wing model, $\alpha = 6.6^{\circ}$.

Figure 1.- Typical shadowgraphs of models in flight at M = 6.0.

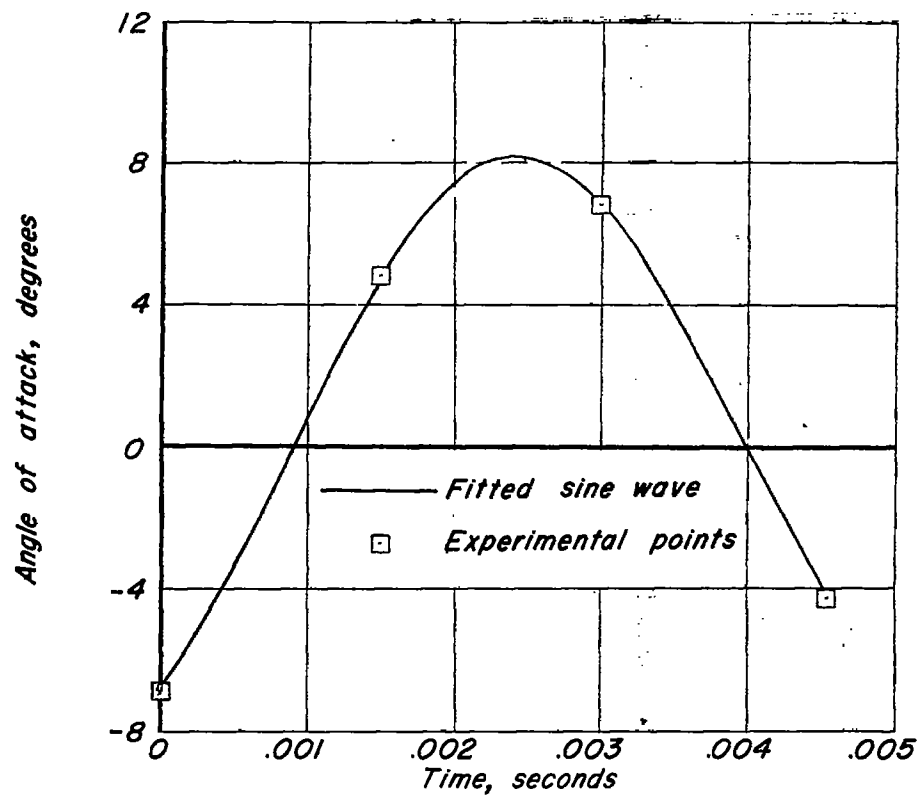

(a) Variation of angle of attack with time.

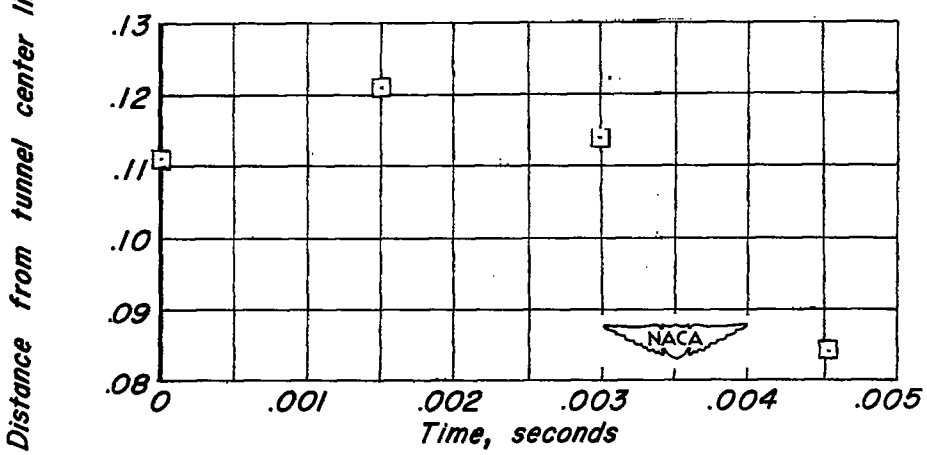

(b) Variation of distance from tunnel center line to model center of gravity with time.

Figure 2.-Time history of model motion.

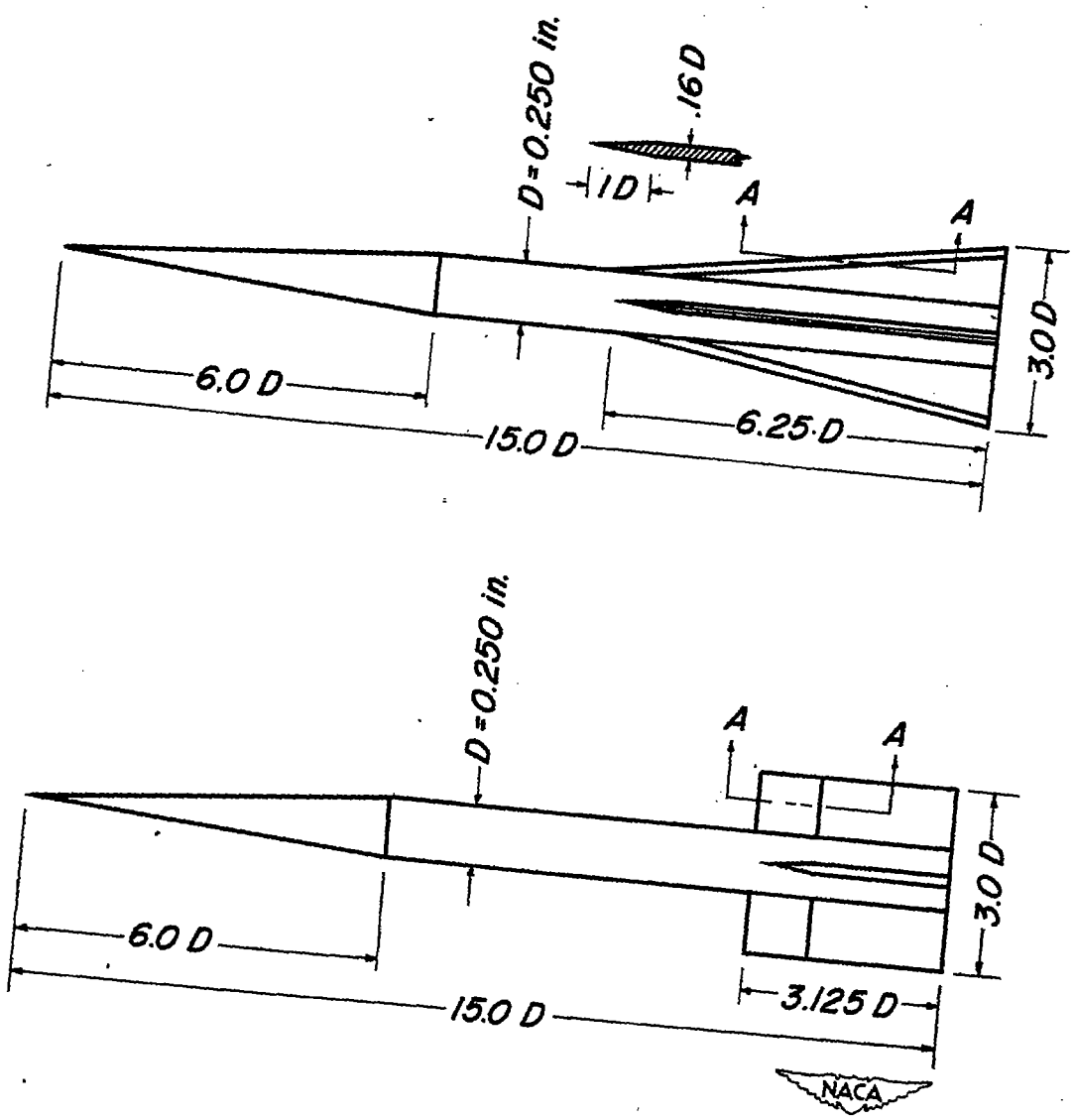

(a) Models.

Figure 3.-Test configurations.

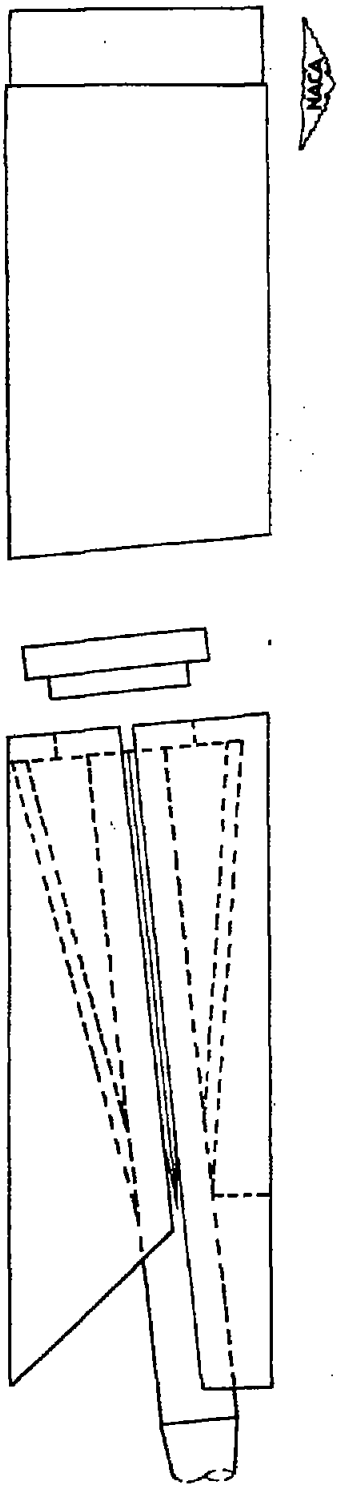

(b) Assembled test round.

Figure 3.- Concluded.

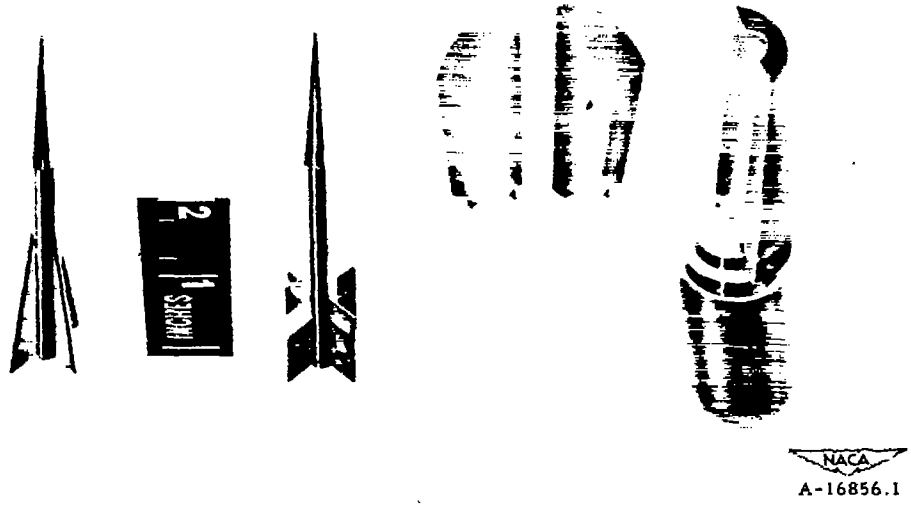

(a) Models and disassembled sabot.

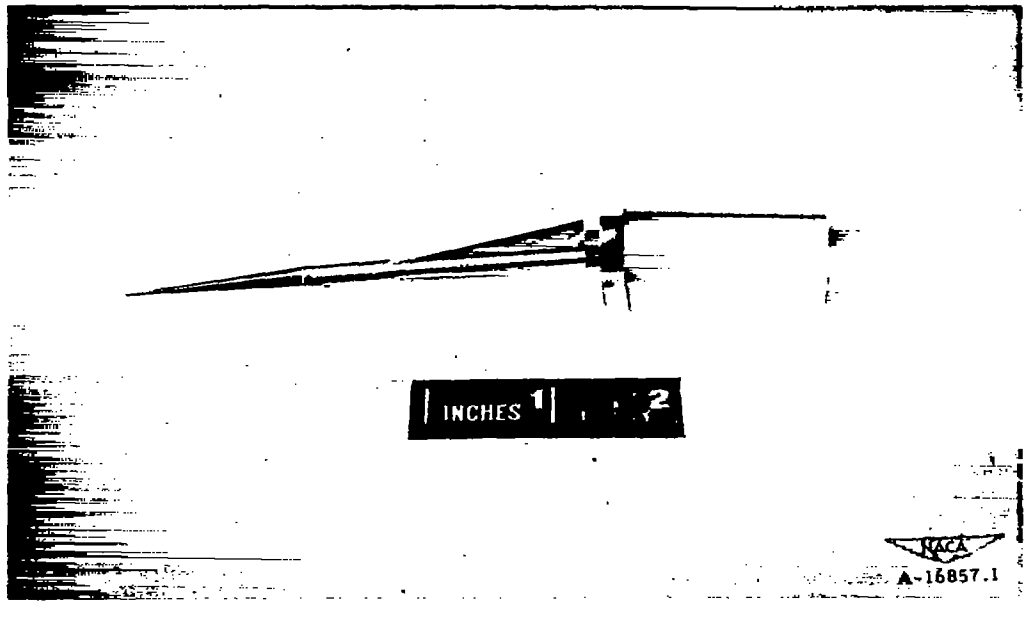

(b) Partially assembled test round.

Figure 4.- Photographs of test configurations.

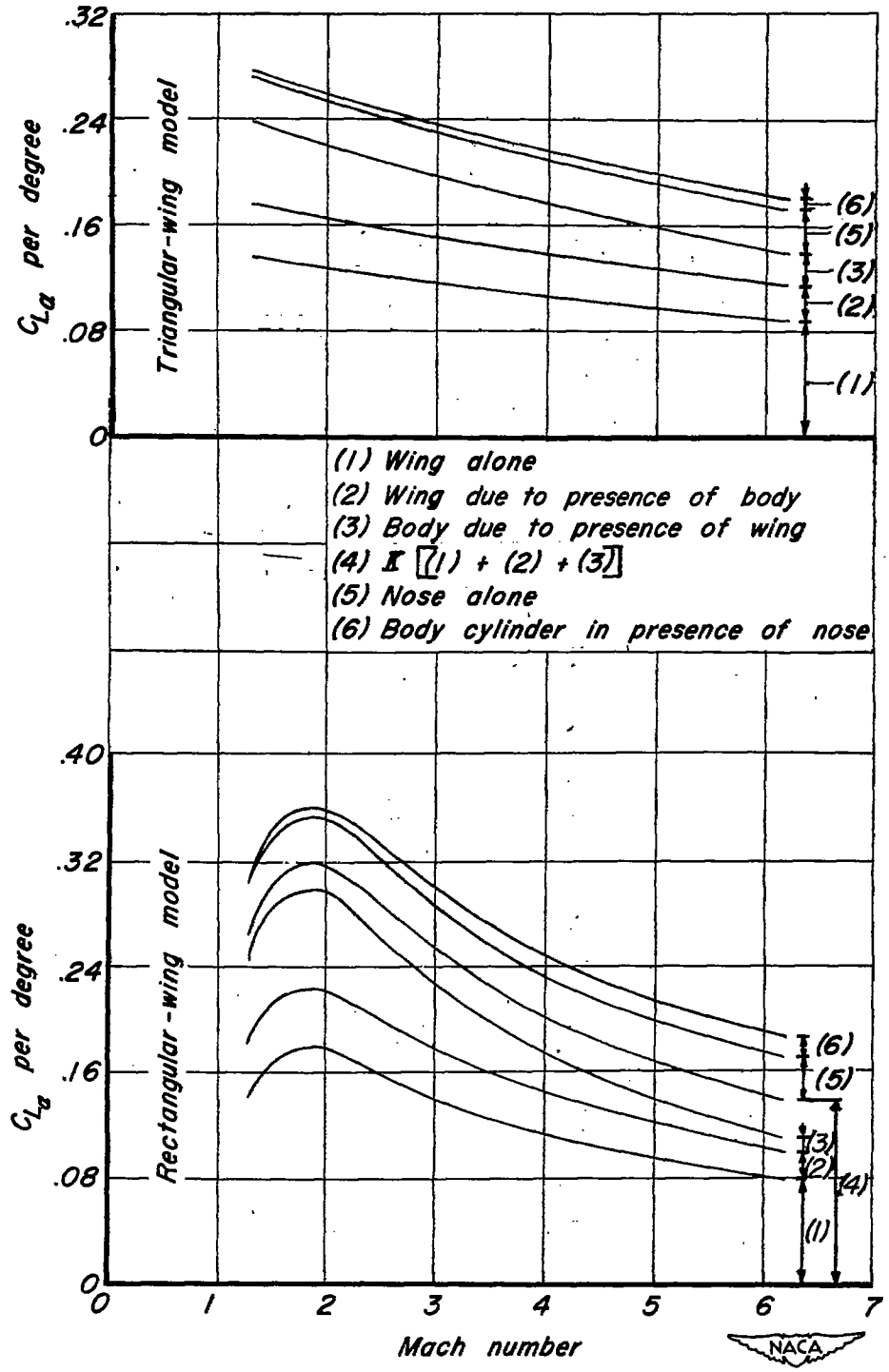

Figure 5.-Lift build-up using modified theory.

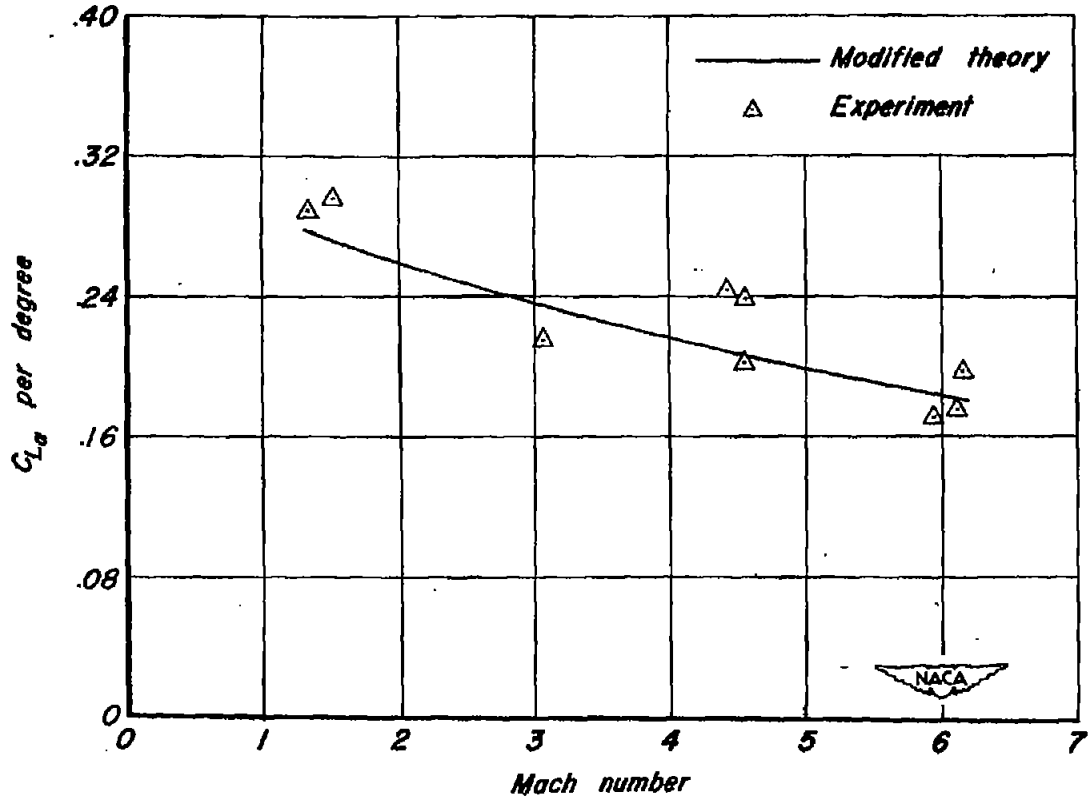

(a) Lateral-movement method.

Figure 6.-Variation of C_{L_α} with Mach number for triangular-wing model.

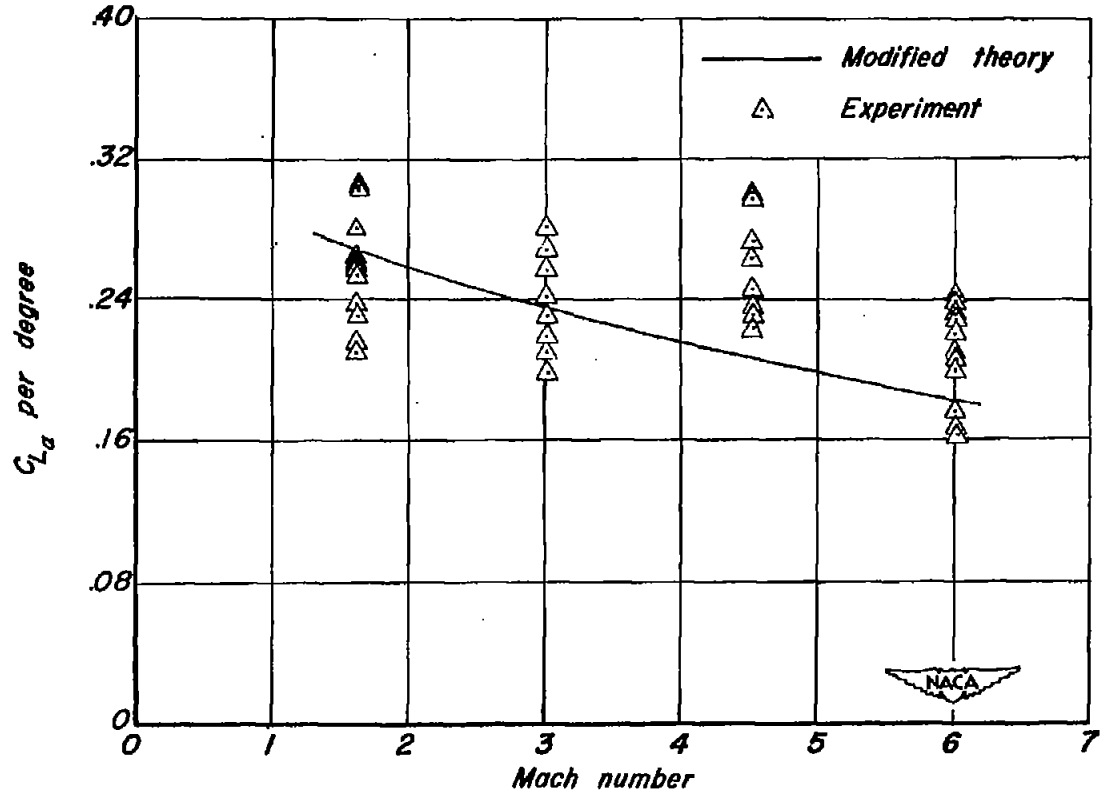

(b) Pitching-moment method.

Figure 6.-Concluded.

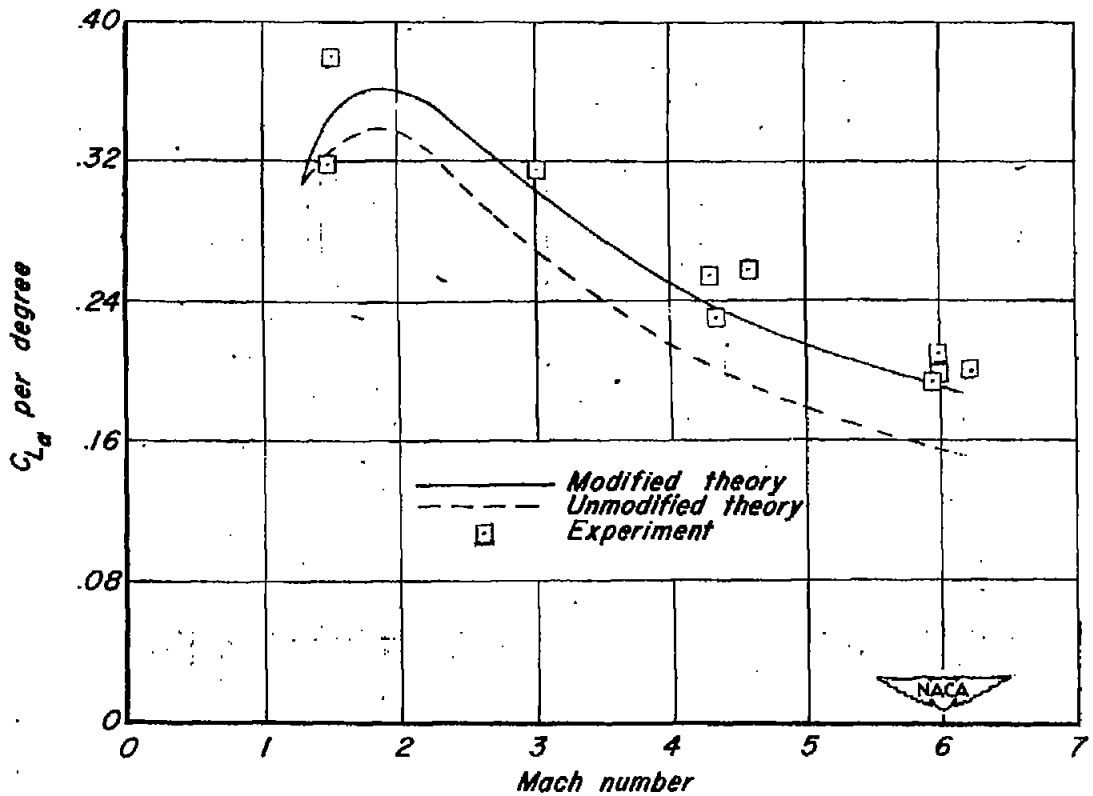

(a) Lateral-movement method.

Figure 7.-Variation of C_{L_α} with Mach number for rectangular-wing model.

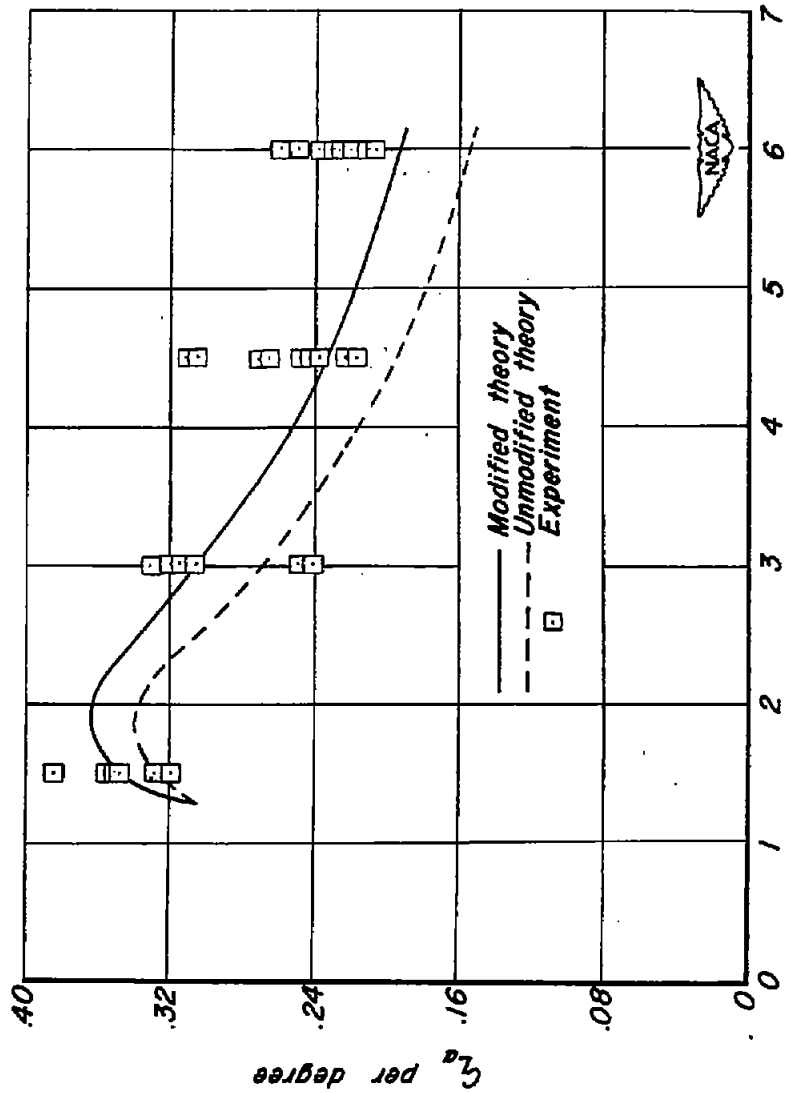

(b) Pitching-moment method.

Figure 7.- Concluded.

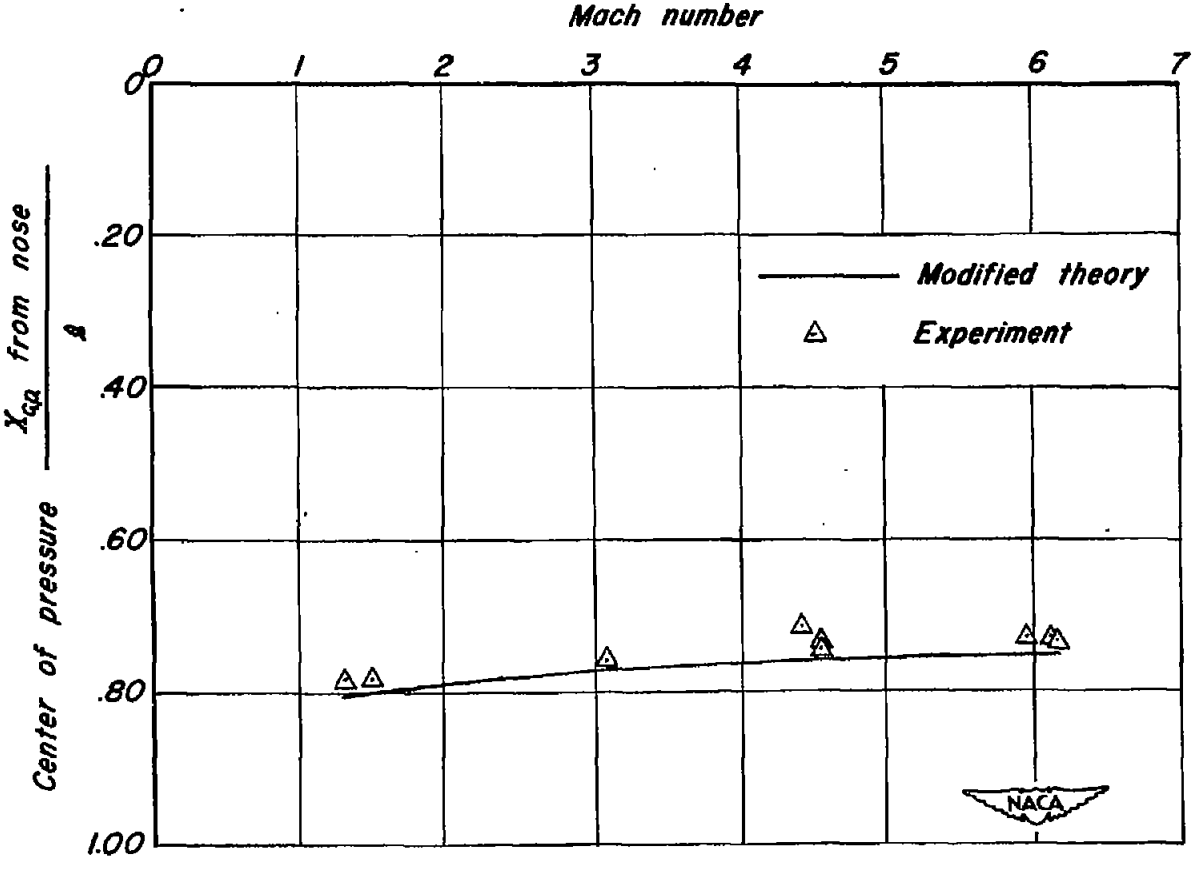

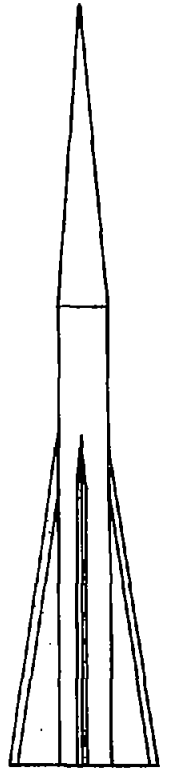

(a) Triangular wing.

Figure 8.-Variation of center-of-pressure location with Mach number.

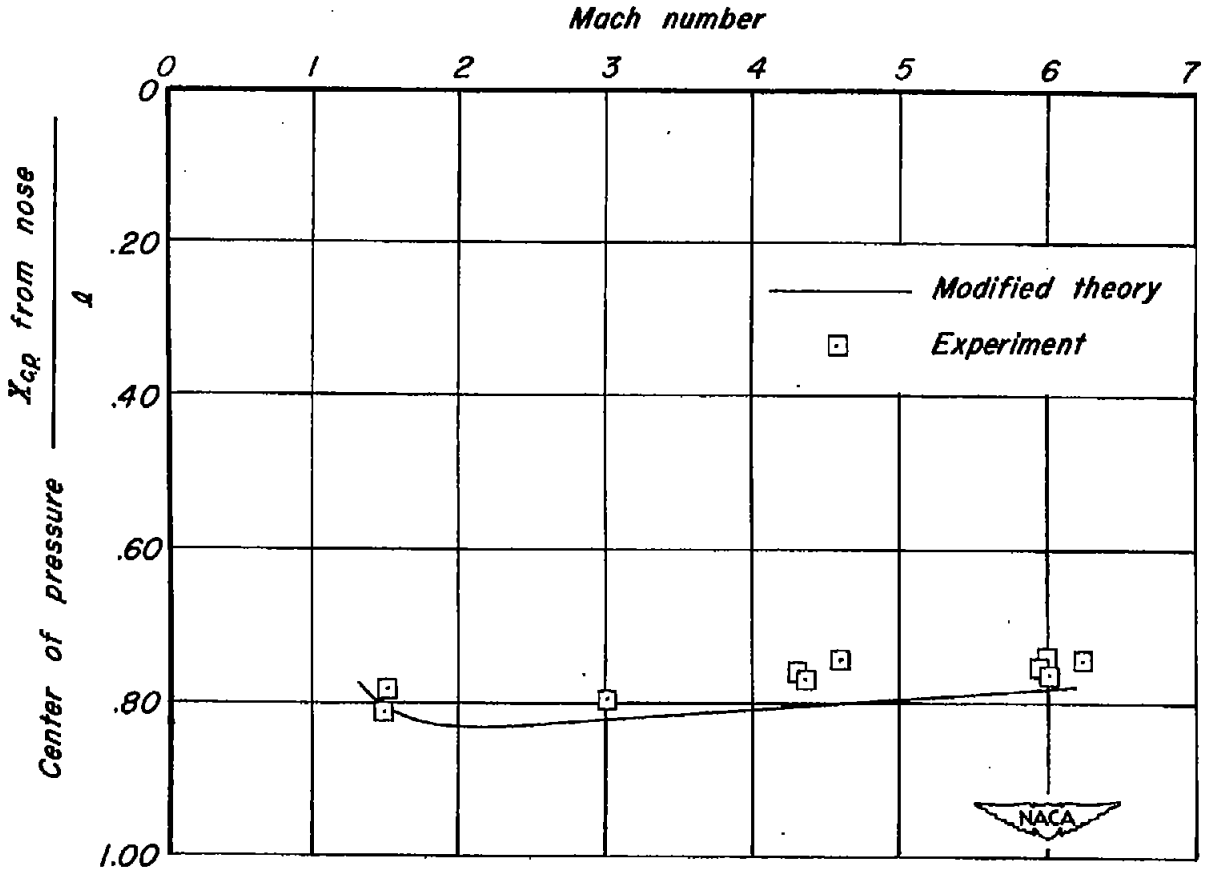

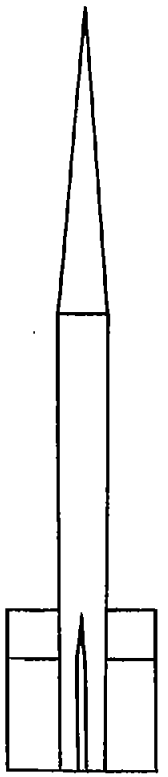

(b) Rectangular wing.

Figure 8.- Concluded.

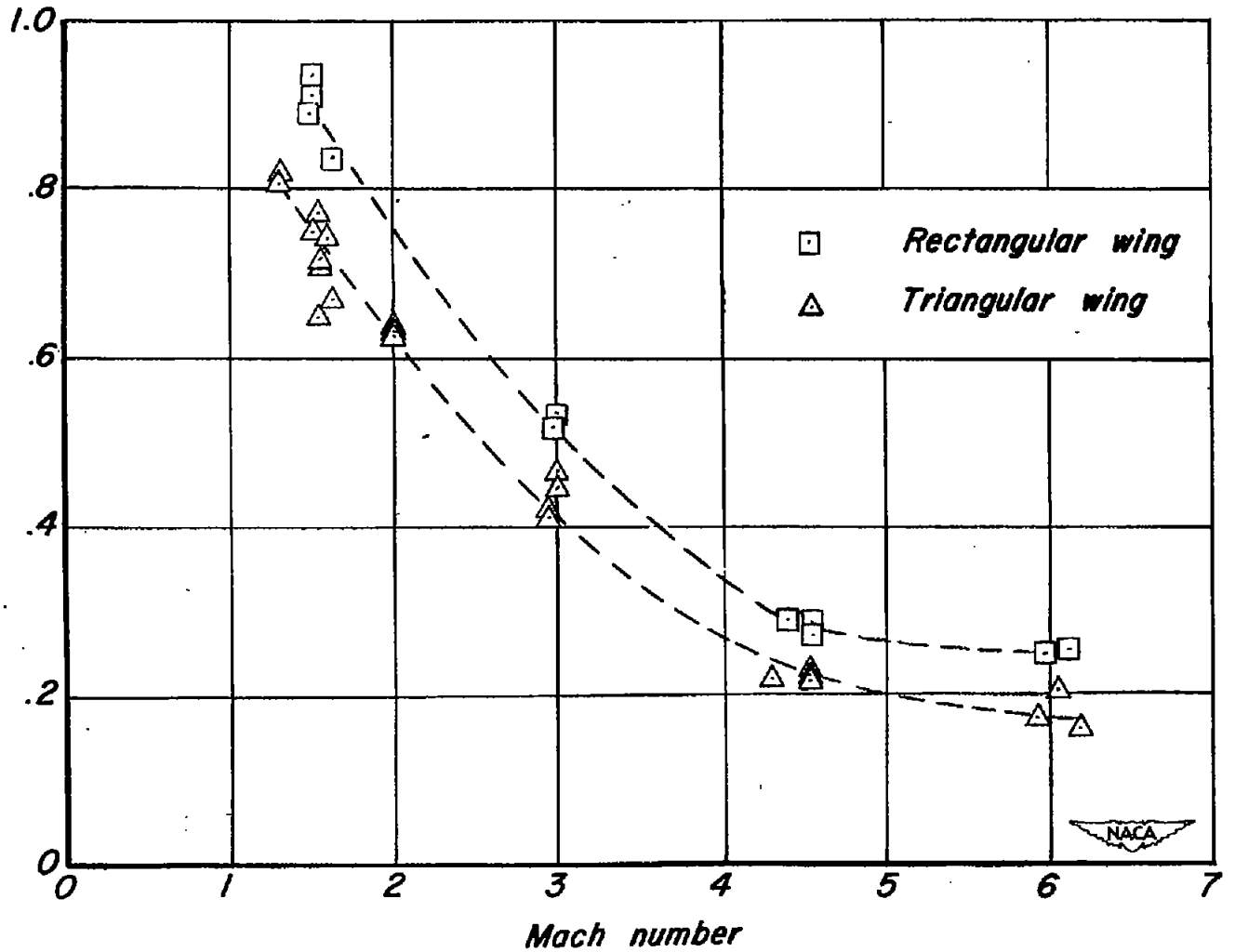

Figure 9.-Variation of drag coefficient with Mach number.